REVIEW ARTICLE

High resolution nonlinear microscopy: A review of sources and methods for achieving optimal imaging

Jeff Squier[a)]
Electrical and Computer Engineering, University of California, San Diego, Urey Hall Addition, MC 0339, 9500 Gilman Drive, La Jolla, California 92093-0339

Michiel Müller
Institute for Molecular Cell Biology, University of Amsterdam, Kruislaan 316, 1098 SM Amsterdam, The Netherlands

(Received 19 December 2000; accepted for publication 23 April 2001)

This article reviews the latest instrumentation used in high resolution nonlinear microscopy and techniques for the temporal and spatial calibration of this instrumentation. This includes an overview of currently available ultrashort laser sources, the dispersion characteristics of microscopes, methods for pulse measurement at high numerical aperture, dispersion compensation techniques, and finally a brief overview of a number of nonlinear imaging methods presently used in these systems. © *2001 American Institute of Physics.* [DOI: 10.1063/1.1379598]

I. INTRODUCTION

Multiphoton laser scanning microscopy has become an important tool for the investigation of biological phenomena where high resolution, three-dimensional imaging is essential for understanding the underlying biological function.[1–3] For example, the fundamental problems in neurobiology are inherently three dimensional: neurons with important micron and submicron sized features are networked in complicated three-dimensional pathways. Scattering by nervous tissue renders ordinary imaging microscopy ineffective except for a select number of preparations. Two-photon laser scanning microscopy makes it possible to produce high-resolution, thin optical sections that can provide complete three-dimensional information of the dendritic tree. The ability of two-photon microscopy to perform functional imaging of neurons even with very thick preparations is thus enabling scientists to measure brain function on specimens that were previously prohibitive.

Two-photon imaging techniques are preferred over single photon methods in this application and others due to several intrinsic advantages which arise as a result of having a nonlinear intensity dependent absorption. For instance, because two-photon absorption is restricted to the focal volume, there is virtually no out-of-focus bleaching. In contrast, single-photon absorption, and the accompanying bleaching process, is quite strong throughout the illuminated volume. In addition, because penetration depth is of fundamental concern, the longer wavelengths, and associated reduced scattering, used in two-photon microscopy extends the usable image depth from tens of microns to several hundred microns. There is also a physiological benefit to the sample that follows from the application of two-photon techniques. In two-photon, the specimen is exposed to wavelengths in the near-IR (as opposed to the green or near-UV used in single photon) that are, in general, considered less likely to reduce cell viability than shorter wavelengths because of the reduced out-of-focus absorption.

The success of two-photon absorption fluorescence has generated substantial interest in the scientific imaging community in further developing and exploiting optical nonlinearities for generating image contrast. Some of these imaging techniques such as second harmonic generation (SHG)[4,5] and coherent anti-Stokes Raman scattering microscopy (CARS)[6,7] have been around for a number of years, but have recently benefited from the development of compact, reliable ultrashort laser sources and are subsequently being looked at with renewed interest. Other techniques such as third harmonic generation (THG) imaging are the result of work in only the past few years,[8,9] but once again have benefited from the fact that it is easier than ever before to generate ultrashort pulses at virtually any desired wavelength.

All of these imaging modalities share a common characteristic: the efficiency of the imaging process scales nonlinearly with the illumination intensity. Thus it is the intent of this article to provide a fundamental review of the basic scientific instrumentation and diagnostics that are available to produce ultrashort pulses, focus them with high spatial resolution, understand the propagation characteristics of a pulse through a high numerical aperture optic, and provide a quantitative measurement of the focused intensity at the specimen plane. These are qualities that are of common interest anytime intensity dependent imaging techniques are used, and are of general concern independent of the particular order of nonlinearity that is being exploited. These parameters deter-

[a)]Electronic mail: jsquier@ucsd.edu

mine the imaging efficiency and resolution, as well as the exposure conditions endured by the specimen.

II. LASER SOURCES FOR MULTIPHOTON IMAGING

The practicality of multiphoton microscopy has as previously mentioned, in no small way, been a result of the dramatic improvement in the quality of the laser sources that are now available. The original two-photon absorption fluorescence work by Denk[1] for instance was performed using a colliding pulse mode-locked dye laser. However, it is difficult to imagine the imaging technique proliferating, despite its obvious utility, had laser technology not evolved beyond the use of dye lasers. Dyes were limiting from several aspects. First, they are toxic and consequently must be handled with great care. Certain dyes aged rapidly, thus the upkeep on the laser could be quite extensive, sometimes requiring weekly dye changes, which also resulted in the generation of substantial toxic waste. These sources lacked the ability to be tuned easily, steps greater than ~30 nm required a complete dye change. The average power of these systems was low, most sources were limited to roughly the 10 mW range.

The capability of ultrashort pulse lasers changed abruptly with the development of high quality Ti:sapphire crystals. The choice of Ti:sapphire as a medium for ultrashort pulse production was a natural one, it could be tuned from 690 nm to greater than 1 μm. This extensive bandwidth (more than an order of magnitude greater than the best dyes) immediately implied the capability of ultrashort pulse production. In addition, a sapphire host meant a mechanically durable laser medium with excellent thermal conduction properties. This, along with the outstanding energy storage characteristics of the gain medium implied significant average powers would be possible. From a practical standpoint, a crystalline host was also much more desirable to handle within the laboratory, no more toxic spills. The potential of Ti:sapphire as an ultrashort pulse oscillator was realized in its present manifestation by Spence *et al.*[10] This work sparked a revolution in solid-state ultrafast oscillators. Within a few years of the Spence paper, average powers of Kerr lens mode-locked lasers reached 1 W, a gain of two orders of magnitude. The tunability of the laser was tested, and it was shown that femtosecond pulses could be produced throughout the gain bandwidth of Ti:sapphire. Finally, the pulse duration also dramatically dropped. It is now relatively straight forward to build a Ti:sapphire laser capable of pulse durations on the order of 10 fs.

Due to its impressive average power capability (up to several watts), broad tuning range (700–1100 nm), and short pulse duration (100 fs or less) Ti:sapphire lasers have become the workhorse of choice for performing multiphoton microscopy. The reliability of the system has also been significantly enhanced with the introduction of all solid-state pump lasers, such as diode-pumped, intracavity frequency-doubled Nd: vanadate lasers. All of these systems are available commercially from a variety of manufacturers. They are extremely robust systems, and have been engineered to the point that someone with little or no previous knowledge in the use of ultrafast lasers can easily operate them.

The average power capability of these lasers makes it possible to drive external frequency conversion devices that further extend the wavelength range of the system. For example, by simply frequency doubling the laser output it becomes an effective blue–green source. Ultrashort Ti:sapphire lasers can also be used to pump optical parametric oscillators extending the wavelength range from ~1.1 μm to wavelengths as long as 2.6 μm. Further, these longer wavelengths can then be doubled, filling the wavelength ''gap'' from 530 to 690 nm that cannot be accessed by either doubling or tuning Ti:sapphire directly. Given all these aspects, it is easy to understand why Ti:sapphire lasers are presently the dominant technology for multiphoton microscopy work. The one inherent drawback for these systems (and ultrafast laser systems in general) however, is cost: a commercial Ti:sapphire system with just the basics goes for over $100 000.00.

Other sources that have proved useful for multiphoton imaging applications include Cr:LiSAF, Nd:YLF, Nd:glass, Cr:fosterite, and fiber-based lasers. Cr:LiSAF has a demonstrated tuning range of 330 nm, from 780 to 1010 nm (peak wavelength is 830 nm) making it very similar to Ti:sapphire. However, practical ultrafast Cr:LiSAF lasers have proven to have a more limited tuning range.[11] Cr:LiSAF has the advantage that it can be directly pumped with presently available diodes. Cr:LiSAF has been primarily implemented in two-photon fluorescence systems imaging everything from neurons[12] to teeth.[13] Cr:LiSGAF has properties (in terms of emission and absorption bands) nearly identical to Cr:LiSAF, but in principle has better power-handling capability for the type of continuous wave operation desired here. Nonetheless, Cr:LiSAF has produced average powers on the order of 500 mW, more than sufficient for most multiphoton imaging applications.[14]

Moving to the longer wavelengths there is Nd:YLF operating at 1047 nm. Wokosin *et al.*[15,16] have used a diode-pumped, picosecond, additive pulse mode-locked Nd:YLF laser for multiphoton fluorescence imaging. This laser is used in conjunction with a fiber/grating pulse compressor to further reduce the pulse width to 120 fs. The narrow bandwidth of YLF restricts the laser from being tuned. At slightly longer wavelengths there are diode pumped Nd:glass lasers operating from 1053 to 1064 nm dependent on the choice of glass.[17] While early Nd:glass lasers produced average powers on the order of 50–100 mW, new designs that meticulously account for the thermal load in the gain media have resulted in average powers of up to 1 W.[18]

For applications further into the infrared, Cr:forsterite operating at 1.259 μm is available. For example, Roberston recently described a 70 fs, Cr:forsterite laser capable of average powers of 700 mW.[19] Clearly, sufficient power for multiphoton imaging.

Finally, there are fiber-based ultrafast laser systems that now cover a broad wavelength range, from 1.03 to 1.55 μm. Using multimode fibers, these lasers have made impressive gains in average power capability[20,21] surging past the 1 W level. The short pulse duration and average power capability of these lasers makes it possible for them to efficiently drive parametric amplifiers further extending their wavelength range.[22] These systems have been used for multiphoton fluo-

rescence and third harmonic generation imaging.[23]

In addition to the broad range of gain media as discussed here, there is a huge array of nonlinear materials available for converting the fundamental laser frequency to higher or lower values. As with the gain media, the variety of materials and techniques is too broad to present in detail in this work; we restrict our attention to a few of the frequency conversion schemes used in our respective laboratories for imaging. For a pump source at 800 nm, an excellent method of converting to higher wavelengths is to use collinear, type II phase-matched BBO.[24] Relatively long crystal lengths can be used in this scheme (since the group velocity mismatch between the signal and pump wavelengths is small) making it possible to produce pulses on the order of 30–50 fs with excellent efficiency. This scheme, combined with additional frequency conversion stages, has produced ultrashort pulses that range in wavelength from 280 nm to 12 μm. Alternatively, noncollinear schemes that use the second harmonic of 800 nm for the pump can be used effectively with type I phase-matched BBO as demonstrated by Wilhelm *et al.*[25] Specifically, Wilhem produced 20 fs pulses over the wavelength range from 470 to 1500 nm using a 2 mm thick BBO crystal.

An important class of nonlinear materials that deserves special mention are quasi phase matched (QPM) nonlinear crystals. By periodically modulating the nonlinear properties of the crystal, phase matching for a broad range of wavelengths can be optimized, ideal for ultrashort pulses. Using periodically poled lithium niobate (PPLN) Galvanauskas *et al.*[22] has shown that it is possible to create a tunable optical parametric generator that requires only 100 nJ of energy in the pump. A 23% conversion efficiency into the signal wavelength at 1.2 μm was achieved using a pump pulse that was 500 fs in duration, centered at 777 nm, with 100 nJ of pump energy. These minimal requirements make it possible to power an optical parametric generator with a system that can operate in the MHz range.

This brief overview has described some of the basic laser choices presently available for performing multiphoton microscopy. In the last part of this section a few different laser architectures that are applicable to virtually all the aforementioned gain media are discussed. These configurations may be useful for further optimization of the imaging system.

A rather straightforward method for increasing the pulse energy by approximately a factor of 10 without the addition of an external amplifier is to cavity dump the oscillator. An outstanding example as to the performance and operation of a cavity dumped Ti:sapphire system is given by Baltuska *et al.*[26] In addition to the energy gain, the use of a cavity dumper enables straightforward control of the repetition rate of the laser. For instance, with a typical cavity dumped Ti:sapphire system the repetition rate can be varied from 1 MHz to 1 kHz at the flip of a switch. This flexibility can be an important consideration for some imaging applications. Finally, cavity dumping can also be applied to optical parametric oscillators with similar gains in energy as demonstrated by Potma *et al.*[27]

In certain cases, a larger gain in energy may be desired.

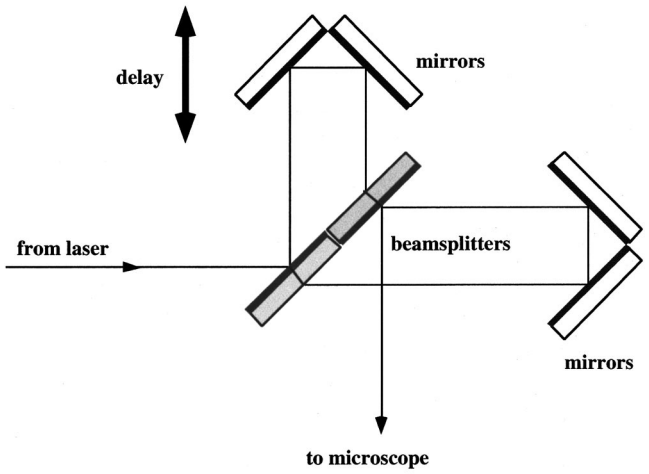

FIG. 1. Basic system for performing autocorrelations.

This means that a chirped pulse amplification (CPA)[28] system is necessary. CPA systems have been made from every type of gain media discussed here. In determining the amplified system that is optimal for a particular need, the ''average power'' rule of thumb is often useful. Essentially all systems, whether oscillators or amplifiers, produce 1 W of average power. Thus if 1 mJ of energy per pulse is required, the system will operate at 1 kHz. Conversely, if a 200 kHz repetition rate is desired, the pulse energy can be expected to be on the order of 5 μJ.

III. MEASURING THE FIELD OF AN ULTRASHORT PULSE AT THE FOCUS OF A HIGH NUMERICAL APERTURE OPTIC USED IN MULTIPHOTON IMAGING

A crucial aspect of multiphoton microscopy is the characterization of the spatial and temporal characteristics of the laser field at the focus of the microscope objective. Detailed knowledge of the field ensures optimum resolution performed with the highest efficiency. In addition, quantitative intensity measurements are necessary for accurately gauging the exposure limits that a living specimen can withstand. In this section a variety of *in situ* methods by which the temporal characteristics of the pulse can be measured are presented. Most importantly, they can be performed at the full numerical aperture (NA) of the objective, which are the conditions under which the system will be used for imaging.

Inherent to virtually all pulse measurement techniques is the necessity of an autocorrelator that is capable of sweeping a time-delayed replica of the pulse across itself. An interferometer designed for making an autocorrelation measurement is shown in Fig. 1.[29] The two arms are perfectly balanced: each pulse travels the same material path length and is subject to the identical number of reflections. By keeping the arms perfectly balanced, the net amount of dispersion due to material and coatings is identical, and a true autocorrelation results. A second important aspect of this autocorrelator geometry is the interferometric aspect. This has the advantage that the beams are fully collinear, and therefore the autocorrelation measurement can be performed at the full NA of the objective.

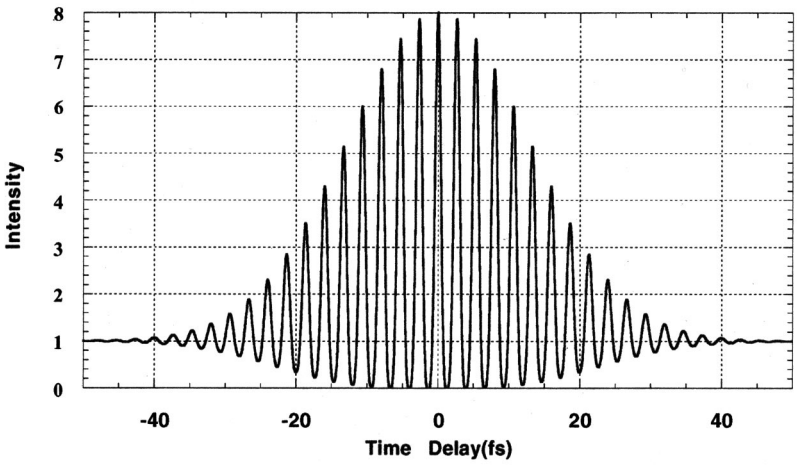

FIG. 2. Calculated second order interferometric autocorrelation for a 20 fs Gaussian pulse.

The beams from the autocorrelator are relayed into the microscope in order that the autocorrelation measurement can be performed at the objective focus. A material capable of generating a nonlinear, intensity-dependent signal is placed at the focus. The intensity-dependent interaction acts as the ultrafast gating function that makes it possible to make a time-dependent measurement of the pulse with a detector that has a frequency response well below that of the optical pulse. At this point a variety of materials/methods are available for the actual pulse measurement, several of the simplest to implement are described here.

A. Two-photon absorption autocorrelation

One of the easiest methods for recording the autocorrelation is to take a small sample of a fluorophore and perform a two-photon absorption autocorrelation (TPAA).[30] The dye should be appropriately mounted to match the imaging conditions under which the objective will be used and care should be taken that the correct immersion medium, coverslip thickness, and mounting medium are in place. Typically a small cell containing dye with these characteristics can be easily fabricated. The action of the two-photon absorption functions as the ultrafast gate that allows the autocorrelation function to be measured with a slow detector such as a photomultiplier tube or photodiode. Figure 2 is an example of what the interferometric autocorrelation trace performed in this manner looks like. The autocorrelation has several distinguishing features that can be used to calibrate the accuracy of the measurement. First, in the absence of aberrations, the ratio of the peak enveloping function to the lower envelope should be 8:1. If this ratio deviates significantly beyond this value the autocorrelator is most likely not aligned properly. Second, the fringe spacing can be used to gauge the time step (based on the wavelength of the laser as measured independently), convenient for deconvolving the final pulse-width measurement. The pulse shown in Fig. 2 is in fact transform limited. In the next section examples of the autocorrelation trace for a pulse with residual higher order dispersion are discussed. Often a second continuous wave laser (such as a HeNe) is directed through the autocorrelator, and the fringes recorded as a function of delay. This provides an accurate and unambiguous determination of the time step.

In order to extract the pulse width, a pulse shape must be determined. In many instances it is sufficient to assume a pulse shape and calculate how well this assumption holds by fitting it to the measured autocorrelation. The most typical pulse shapes are either Gaussian or hyperbolic secant squared. A more rigorous approach is to first measure the pulse spectrum. By Fourier transforming the spectrum (and assuming flat spectral phase) the transform limited pulse shape can be determined. The autocorrelation function can then be calculated and again compared to the measured autocorrelation. This approach is highly recommended as it provides a yardstick as to the best performance (in terms of pulse width) that can possibly be expected from the laser system. Also, spectral measurements performed at the input and output of the microscope can be especially useful, as any spectrally limiting components that may limit the pulse width of the system can be identified.

Spatial information can also be extracted from this apparatus. By blocking an arm of the autocorrelator, and scanning the sample in the z direction, a sectioning measurement can be performed. This can be especially useful in determining if the beam is appropriately filling the objective so that the full NA of the system is being used. This single simple apparatus thus makes it possible to do a very nice spatial and temporal characterization of the beam focus that is adequate for many applications.

B. Two-photon absorption in photodiodes

A disadvantage of using a fluorophore for performing TPAA is the limited bandwidth. Typical dyes have bandwidths on the order of 30 nm, meaning that a new dye is necessary should the laser be tuned beyond this limit. A more achromatic alternative is to use the two-photon response of GaAsP photodiodes.[31] These diodes have been shown to have a spectral response in the range of 720–950 nm that is more uniform than many types of doubling crystals used in typical autocorrelation measurements. The actual two-photon response for these diodes covers the range of 600–1360 nm, completely encompassing the entire tunability range of femtosecond lasers like Ti:sapphire that are typically used in multiphoton microscopy. In addition, these diodes are extremely robust and inexpensive, making them a near ideal choice for autocorrelation measurements. Millard

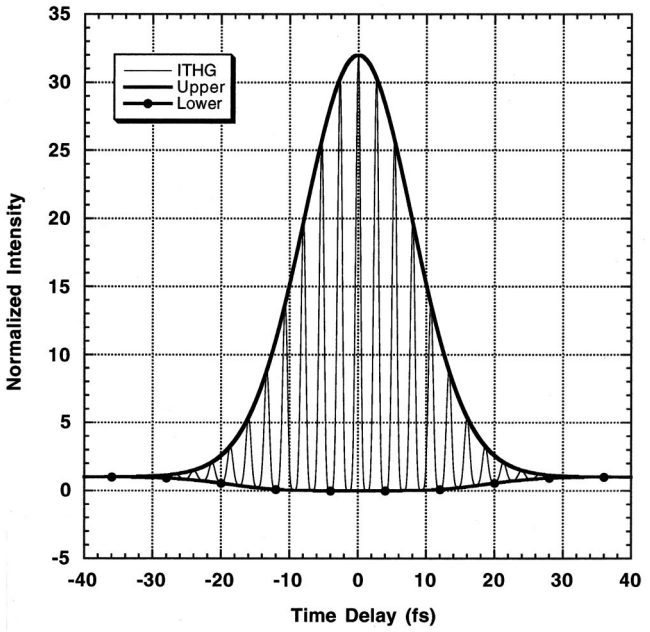

FIG. 3. Calculated third order interferometric autocorrelation for a 20 fs Gaussian pulse.

et al.[32] demonstrated how such diodes are easily implemented in the microscope, and, as with TPAA, they can be used for spatial sectioning measurements as well. The autocorrelations taken with GaAsP photodiodes show a superior signal-to-noise ratio compared to TPAA measurements as well.

Similarly Jaspara *et al.*[33] have used two-photon current generation in ZnSe to perform autocorrelation measurements of pulses at high numerical aperture. In particular, they obtained autocorrelation widths of 9.0 fs for a slightly underfilled 100×/0.85 NA Zeiss objective.

C. Third harmonic autocorrelation

A third alternative is to generate third harmonic at the coverslip interface, and use this signal to perform the autocorrelation.[34] Interferometric intensity autocorrelations generated in this manner have several advantages. First, no special materials are needed, the glass coverslip is the nonlinear medium. It is achromatic, autocorrelations using this method have been performed from 800 to 1500 nm.[35,36] This technique is especially useful for very short pulses, as group velocity mismatch considerations across the interface are negligible. As this is a third order process, the autocorrelation envelopes do not follow an 8:1 contrast as in our previous examples, but rather they are 32:1. A typical interferometric, third order intensity autocorrelation is shown in Fig. 3.

In each of these examples a method is described wherein the pulse duration at the focus of the objective can be measured. This information, while valuable, does not in fact provide an unambiguous, and therefore complete characterization of the pulse temporal profile. Certain applications may require knowledge of the pulse phase, which cannot be determined by any of the measurements described to this point. Full pulse characterization requires a more sophisticated

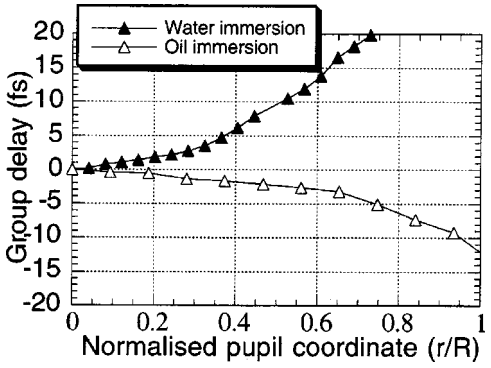

FIG. 4. The radially varying time-of-flight error measured as a function of input radius for an oil immersion and water immersion objective.

measurement such as frequency resolved optical gating (FROG).[37] The basic phase retrieval technique involves spectrally resolving the autocorrelation. This can be accomplished, for instance, by placing a spectrometer between the output of the autocorrelator and the detector. A high numerical aperture FROG technique has been demonstrated recently by Fittinghoff *et al.*[38] and used to characterize 22 fs pulses at the focus of a 1.2 NA objective. This method makes it possible to determine the intensity profile and phase of the pulse. Such a scheme is nontrivial to implement, and should only be considered if phase information is critical for the imaging application.

D. Radially varying propagation time delay

One factor affecting each of the aforementioned measurement techniques is radially varying time-of-flight errors.[39] When using refractive optics, it is important to note that the net group delay for those rays traveling along the center of the optical path may vary from those off-center. This radially varying time-of-flight error manifests itself in several ways in the autocorrelation measurement. First, the envelopes which define the interferometric autocorrelation traces deviate from the standard 8:1 or 32:1 contrast ratios. This is due to a mixing of collinear and noncollinear autocorrelation functions produced by the radially varying time-of-flight error. Second, the pulse duration also becomes a function of pupil position as a result of this phenomena, and the autocorrelation measurement convolves this varying pulse duration information in a complicated way. The radially varying time-of-flight errors vary from objective to objective. Figure 4 shows the time-of-flight error measured relative to the central ray of the system for an oil immersion objective and a water immersion objective. Several groups have employed various interferometric techniques[33,40] for measuring the group delay and group delay dispersion as a function of aperture.

IV. DISPERSION IN MULTIPHOTON IMAGING SYSTEMS

Clearly in dealing with ultrashort pulses, dispersion of the optical glasses and dielectric coatings that the pulse passes through or reflects from is an important consideration. Important from at least two aspects: the efficiency of the

multiphoton process and the damage threshold of the specimen. Without due consideration of the microscope's dispersive properties, neither of these aspects of multiphoton imaging can be adequately addressed.

First consider the average power of the detected signal, assuming two-photon absorption fluorescence as the imaging modality. While the instantaneous signal scales as the square of the excitation intensity, and hence depends inversely on the square of the pulse width, the detected integrated signal power scales inversely with the pulse width to the power of unity. Thus a 1 ps pulse produces a signal that is ten times smaller than a 100 fs pulse of equal energy. The typical optical path lengths found in microscopes provide sufficient dispersion that 100 fs pulses can be stretched by up to a factor of 2, reducing the excitation efficiency by the same factor of 2. For higher order processes, such as third harmonic generation or three photon absorption, this becomes even more significant. A pulse stretched by a factor of 2 reduces the detected signal by a factor of 4.

Dispersion in multiphoton imaging systems is most conveniently discussed quantitatively in terms of the spectral phase, $\varphi(\omega)$, of the pulse. A transform limited pulse corresponds to a flat spectral phase, all the frequency components arrive simultaneously resulting in a pulse duration and a pulse structure that is completely determined by the width and shape of the pulse spectrum. In propagating from the laser to the focus of the objective the spectral phase can be significantly distorted resorting in pulse broadening and temporal pulse structure. Thus while the pulse is being focused spatially, temporally it is becoming ''defocused.'' Obviously, in imaging applications where the contrast is highly nonlinear with intensity it is desirable to avoid temporally stretching the pulse in this manner.

A useful method for determining the extent of temporal reshaping is to begin by expanding the pulse spectral phase $\varphi(\omega)$ in terms of a Taylor series.

$$\varphi(\omega)=\varphi(\omega_o)+\left(\frac{d\varphi}{d\omega}\right)_{\omega_o}(\omega-\omega_o)+\frac{1}{2!}\left(\frac{d^2\varphi}{d\omega^2}\right)_{\omega_o}\times(\omega-\omega_o)^2+\frac{1}{3!}\left(\frac{d^3\varphi}{d\omega^3}\right)_{\omega_o}(\omega-\omega_o)^3+\frac{1}{4!}\left(\frac{d^4\varphi}{d\omega^4}\right)_{\omega_o}(\omega-\omega_o)^4+\cdots. \tag{1}$$

In general, the coefficients in the series are found by calculating the net optical path length through the material(s) of interest and evaluating the appropriate order derivative at the central wavelength:

$$\mathrm{GD}=\varphi_1=\frac{L}{c}\left[n(\lambda_0)-\lambda_0\left(\frac{dn}{d\lambda}\right)_{\lambda_0}\right], \tag{2a}$$

$$\mathrm{GDD}=\varphi_2=\frac{1}{2!}\frac{L}{c}\left(\frac{\lambda_0}{2\pi c}\right)\left[\lambda_0^2\left(\frac{d^2n}{d\lambda^2}\right)_{\lambda_0}\right], \tag{2b}$$

$$\mathrm{TOD}=\varphi_3=\frac{1}{3!}\frac{L}{c}\left(\frac{\lambda_0}{2\pi c}\right)^2\left[3\lambda_{0s}^2\left(\frac{d^2n}{d\lambda^2}\right)_{\lambda_0}+\lambda_0^3\left(\frac{d^3n}{d\lambda^3}\right)_{\lambda_0}\right], \tag{2c}$$

$$\mathrm{FOD}=\varphi_4=\frac{1}{4!}\frac{L}{c}\left(\frac{\lambda_0}{2\pi c}\right)^3\left[12\lambda_0^2\left(\frac{d^2n}{d\lambda^2}\right)_{\lambda_0}+8\lambda_0^3\left(\frac{d^3n}{d\lambda^3}\right)_{\lambda_0}+\lambda_0^4\left(\frac{d^4n}{d\lambda^4}\right)_{\lambda_0}\right]. \tag{2d}$$

It is possible to develop an intuitive understanding for how a particular order will effect the pulse shape by assuming a spectral shape, multiplying by a spectral phase weighted by the desired order, and transforming to the time domain. What is immediately apparent is that only second order and higher terms are responsible for distorting the pulse shape. The second order coefficient is often referred to as the group delay dispersion (GDD), and results in broadening the pulse width whenever it is nonzero. The third order dispersion (TOD) distorts the pulse shape asymmetrically. The asymmetry can be reversed by flipping the sign of the TOD. In microscopy, most applications require only consideration through third order. Quartic phase limited performance of the system is usually sufficient.

For a Gaussian pulse shape, it is quite straightforward to derive the following simple analytic expression that calculates the pulse width for a given amount of GDD:

$$\tau_{\mathrm{stretched}}=\tau_{\mathrm{initial}}\left[1+\left(\frac{\varphi_2 4\ln 2}{\tau_{\mathrm{initial}}}\right)\right]^{1/2}. \tag{3}$$

The dispersion of typical objectives has been measured by several groups.[41,42] From these measurements broadening of femtosecond pulses can be estimated. Consider a 100 fs pulse, at 800 nm, typical pulse parameters used in multiphoton imaging. The measured group delay dispersion (GDD) ranges from 580 to 1200 fs^2 for standard objectives. The net dispersion of the microscope (including beam expanders, filters, and dichroics) can then be on the order of 4500 fs^2. This amount of dispersion broadens a 100 fs pulse to ~270 fs, significantly impacting the efficiency of any nonlinear imaging process. (Note: one extremely confusing aspect in the literature is the weight given to each of the terms in the Taylor series. This is not uniform within the literature by any means, and with each paper care must be taken to sort out exactly how the GDD or higher order terms are weighted in order to properly calculate the spectral phase.)

The dispersion produced by the microscope can be precompensated through a variety of means. A grating pair or prism pair arranged to provide negative GDD are the most common means of dispersion precompensation. Gratings have the advantage of high dispersion, making the system very compact, whereas prisms have the advantage of high efficiency. A second advantage of prisms over gratings is the sign of the third order dispersion (TOD), which is negative for prisms and positive for gratings. Thus the higher order dispersion for a prism system is opposite to that of the glass material that is being compensated, whereas the grating's TOD adds to the TOD of the glass. Ultimately it is the re-

sidual higher order dispersion from the compressor that in fact limits the pulse width. Careful attention to the higher order terms is obviously necessary to ensure optimum compensation.

While the prism pair is better matched with respect to balancing the higher order dispersion than a grating pair, care must also be taken with regards to the type of glass used in the prism sequence. SF10 glass is often used since it is highly dispersive and a compact compensator can be designed around this choice. However, as shown by Müller *et al.*,[41] such dispersive glasses result in high residual TOD that can limit pulse compression. Fused silica is a better glass choice when either the shortest pulse widths or greatest wavelength tunability is desired. Pulses as short as 15 fs have been generated at the focus of high NA optics using this type of sequence. The pulse width in this case is still limited by the residual TOD of the prism sequence. Jaspara has demonstrated pulses as short as 9 fs by further balancing of this residual TOD through the use of dielectric mirror coatings.[33]

A novel method for compensating for GDD and TOD in the correct proportion is through the use of ''grisms.'' Essentially, these are gratings written onto prisms. The advantage is that the ratio of third order compensation to second order can be precisely engineered to be opposite in sign, and equal in magnitude to that of the glass in the microscope. This means that the compressor precisely compensates for the GDD and TOD of the system, and only the FOD remains uncompensated. Kane *et al.*[43] has demonstrated that it is possible to pass a 100 fs pulse centered at 800 nm through 100 m of fiber and fully compensate for the dispersion of the fiber[44] to fourth order. In addition to having the correct magnitude and sign of dispersion, the grisms are extremely dispersive, making very compact dispersion compensation systems possible. For the typical amounts of dispersion found in a microscope, a grism pair will only require millimeter separations (compared with meter separations for a fused silica prism sequence). In addition, long fiber optic delivery systems should be possible using this technology. This would make it possible to feed many imaging systems from a single, centrally located oscillator.

Finally it should be noted that the dielectric coatings of many commonly used mirrors in multiphoton microscopes can be highly dispersive, especially as the pulse width drops below 50 fs. In a work by Knox *et al.*[45] a very straightforward method for precisely measuring the dispersion of coatings is presented. The white light interferometric technique discussed by Knox *et al.* is a highly useful method for characterizing the dispersive effects of common coatings found in a microscope.

V. BALANCING THE LASER PARAMETERS

An increasing number of studies have addressed the issue of biological damage in multiphoton microscopy. This in itself is a complicated issue because of the large number of parameters involved (laser power, pulse energy, pulse duration, wavelength, dwell time, specimen related conditions, etc.). However, a number of general observations are consistently observed in various studies.

Photo-induced biological damage appears to be a threshold phenomenon.[46] The threshold is generally found to be wavelength dependent, with reduced damage at longer wavelengths. For instance, in one study a 50% cloning efficiency of CHO cells was observed at power levels of 2.5 and 6 mW for a two-photon excitation wavelength of 780 and 920 nm, respectively (Ti:sapphire laser: 240 fs, 80 MHz).[47] The precise damage mechanism is as yet unclear.

Multiphoton experiments have almost exclusively been performed with near infrared (NIR) lasers, especially Ti:sapphire (700–1100 nm) and Nd:YLF (1047 or 1053 nm). Since water absorption increases significantly at longer wavelengths in going from the visible to the NIR region of the spectrum,[48] biological damage through heating can be expected. However, careful calculations have shown that this is generally not significant under typical experimental conditions.[49] Since, in addition, biological specimen are virtually nonabsorbing in the NIR (in the absence of hemoglobin, melanin, or chlorophyll), photothermal induced damage through linear (i.e., one-photon) absorption is unlikely. This has been confirmed by the observation of reduced biological damage for an excitation wavelength of 920 nm relative to that at 780 nm, despite a sevenfold increase in water absorption in going to the longer NIR wavelength.[47]

A more likely damage mechanism is through multiphoton absorption of endogenous cellular components, such as NAD(P)H, flavins, porphyrins, DNA, and proteins. This can in turn lead to the production of oxygen radicals. The fact that the damage process is itself multiphoton induced is substantiated by monitoring cell viability as a function of pulse duration.[47] At shorter wavelengths, such as excitation at visible wavelengths as in regular confocal microscopy, oxidative stress may also be induced through linear absorption.[50]

In biological applications, the damage mechanism is subtle and only partially understood. Clearly it is limited because of the absorption of light, either in a single photon or multiphoton process. In parametric nonlinear optical processes, i.e., in which there is no net transfer of energy from the light field to the specimen, the upper damage limits may be quite different. In this case, the primary limitation is laser-induced breakdown.

For ultrashort pulses, the mechanism of laser-induced breakdown is as follows. Multiphoton absorption (up to seventh order) causes highly localized plasma formation. The rapid expansion of the plasma causes a microexplosion that results in observable damage. The created ''damage structure'' is considered to be due to either a small change in refractive index or a vacuum bubble.[51]

Laser-induced breakdown is a threshold phenomenon. For transparent media and ~100 fs pulses, the laser-induced breakdown threshold is found to be ~60 nJ/pulse.[52] In third-harmonic generation imaging experiments a similar threshold was observed for a transparent specimen.[53] For a biological specimen the upper limit for laser-induced damage to the specimen is lower (~1–10 nJ/pulse),[9,54] being limited in this case by competing multiphoton absorption processes of the laser light at the fundamental frequency.

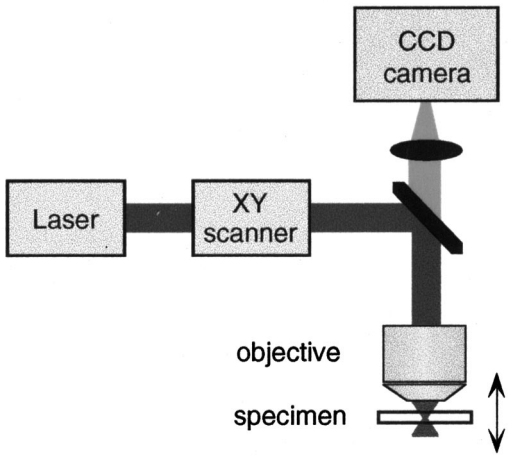

FIG. 5. Generalized schematic of a two-photon absorption microscopy setup. A microscope objective focuses the laser pulses onto the specimen. The specimen is raster scanned in a point excitation mode, generally using mirror scanning for the *X* and *Y* directions and specimen scanning for the *Z* direction. The fluorescence is detected in the backscattering direction and may be imaged directly onto a CCD camera.

VI. THE BASIC INSTRUMENT

Various configurations have been used in multiphoton absorption microscopy. In all cases either laser scanning or specimen scanning is required. This can be accomplished in several ways: by adaptation of a confocal microscope retaining the descanned detection channel; by use of laser scanning optics and a specific detection channel without descanning optics and optimized for fluorescence collection efficiency; or by using laser scanning optics in combination with widefield charge coupled device (CCD) detection. In general a specifically optimized microscope configuration is required to take full advantage of the various features of multiphoton absorption microscopy. A schematic of a typical two-photon microscope setup is depicted in Fig. 5.

Typically, in high resolution biological applications, power levels not exceeding ~100 pJ/pulse should be used to retain cell viability. On the other hand, ultrashort lasers routinely produce power levels well over 10 nJ/pulse. Thus ample power is available for parallel excitation to speed up the image acquisition process. The first approach used in this respect was based on the use of line, rather than point, excitation, in combination with widefield CCD detection.[55] This provides real-time image acquisition rates at the expense of a reduced axial resolution. For example, for a numerical aperture of 1.3 an optical sectioning resolution of ~5 μm results in line scan mode,[55] as opposed to ~1 μm axial resolution that is attainable in point-scanning mode.[56]

A more ideal way of spreading the available excitation power over the sample is the simultaneous use of several well separated foci, each of diffraction-limited quality.[57] In this way it is possible to retain the optimal axial resolution. In combination with a simple and efficient detection scheme, such as a CCD detector which views the whole field in parallel, image acquisition rates can be strongly enhanced.

In the first applications of this concept,[58,59] several tens of diffraction-limited foci have been produced in a two-photon absorption microscope using micro-lenslet array elements. The spacing between the foci has to be chosen carefully. If the foci are too close to one another, the sectioning resolution diminishes through out-of-focus interference. On the other hand, spreading the foci too far apart reduces the efficiency of excitation over the whole field-of-view.

Recently it was demonstrated[60,61] that by introducing time delays between the different foci by an amount larger than the pulse width, the various excitation spots can be positioned arbitrarily close with respect to each other, without loss in resolution.

Finally, it should be mentioned, that adaptive optics can also be employed to help optimize resolution. Recently, several groups have implemented adaptive correction to multiphoton imaging schemes.[62–64]

A. Resolution of an ultrashort pulse microscope

The resolution of any microscope in general, and that of an ultrashort optical microscope in particular, is not easily defined in general terms. Various criteria have been used either in terms of the apparent spreading of the image of an infinitely small point object, the capability to discriminate two separated point objects, or, alternatively, in terms of the frequency bandpass of the optical system. Since a detailed description of all aspects involved is outside the scope of this work, the discussion here is restricted to the effective three-dimensional size of the interaction volume in an ultrashort pulse microscope. This interaction volume is determined, not only by the focusing properties of the microscope objective, i.e., by its numerical aperture and the wavelength, but also by the order of nonlinearity of the interaction. In addition, confocal detection can effectively reduce the observation volume.

B. The Rayleigh criterion

The optical resolution is traditionally defined through the Rayleigh criterion, which states that two components of equal intensity should be considered to be just resolved when the principle intensity maximum of one coincides with the first minimum of the other.[65] In the classical description of the focal field produced by a high numerical aperture lens, both Kirchhoff, Debye, and paraxial approximation are imposed and dimensionless optical coordinates are introduced:

$$\nu = r\frac{2\pi}{\lambda m}\sin\alpha, \quad u = z\frac{2\pi}{\lambda_m}\sin^2\alpha, \tag{4}$$

where r and z are the radial and axial coordinate, respectively, and $\lambda_m = \lambda/n$ is the wavelength of the optical field in the medium with refractive index n. In this description the intensity distribution near the focal point for an optical field with a constant amplitude across its wave front has an analytical solution in the form of the Lommel functions.[65,66] The intensity distribution of the focal field in a plane coinciding with the focal point and orthogonal to the optical axis is given by

$$I(0,\nu) \propto \left|\frac{2J_1(\nu)}{\nu}\right|^2, \tag{5}$$

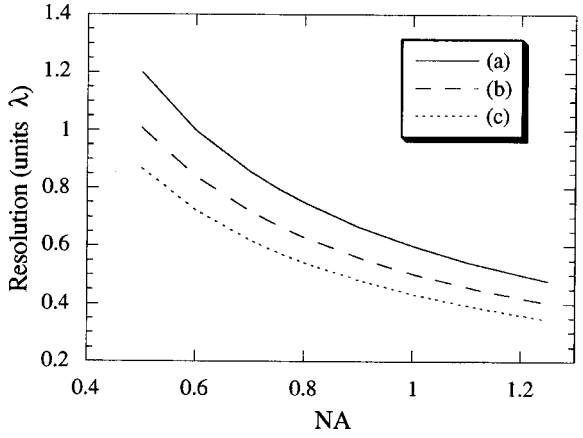

FIG. 6. Lateral resolution of an optical microscope as a function of numerical aperture (NA) based on (a) the lateral position of the first node of the focal field distribution (Rayleigh criterion); or as the FWHM of the lateral focal field distribution in the focal plane from (b) classical theory and (c) full diffraction theory.

where $J_1(\nu)$ is the first-order Bessel function of the first kind. Similarly, the intensity distribution along the optical axis is described by

$$I(u,0) \propto \left(\frac{\sin(u/4)}{u/4} \right)^2. \tag{6}$$

The first node in these lateral and axial distributions is at $\nu_0 = 1.22\pi$ and $u_0 = 4\pi$, respectively, in optical coordinates. In real units the first nodes are thus found at

$$r_0 = \frac{0.61 \cdot \lambda}{NA} \text{ and } z_0 = \frac{2 \cdot n \cdot \lambda}{(NA)^2}. \tag{7}$$

For convenience, it is often assumed that the full-width-at-half-maximum (FWHM) of these distributions is approximately equal to the distance to the first node, i.e., $\text{FWHM}_{\text{lateral}} \approx r_0$ and $\text{FWHM}_{\text{axial}} \approx z_0$. In fact the FWHM is only ~85% of this value. Nevertheless, Eq. (7) is generally used to describe the diffraction limited focusing properties of a high numerical-aperture microscope objective and, subsequently, of the optical resolution through the Rayleigh criterion. Note that the imposed approximations are not strictly valid for high numerical aperture focusing. Full diffraction theory calculations[66] predict even smaller values for the FWHM of the focal field distributions than those based on the classical theory (Fig. 6).

C. The nonlinear interaction volume

In general, the influence of a signal response that depends nonlinearly on the input intensity is to reduce the effective interaction volume and thus increase the resolution, relative to its linear counterpart. Let us assume that the contrast in the microscope depends on the focal field intensity to the power N. To evaluate the influence of the nonlinear interaction on the effective interaction volume consider a general Gaussian distribution

$$I(x) = \exp(-x^2/2\sigma^2), \tag{8}$$

for which the FWHM is at

$$\text{FWHM} = 2\sigma\sqrt{-2\ln\tfrac{1}{2}}. \tag{9}$$

It follows that for a Nth order process the FWHM reduces to

$$\text{FWHM} = \frac{1}{\sqrt{N}} 2\sigma\sqrt{-2\ln\tfrac{1}{2}}. \tag{10}$$

Hence in general the interaction volume of a Nth order nonlinear process decreases by a factor of $\sqrt{N}$, relative to the linear interaction volume at the same optical wavelength. This is true for, for instance, four-wave-mixing processes. However, in multiphoton absorption processes, excitation of the one-photon equivalent electronic transition of the fluorophore requires a longer wavelength that scales with the nonlinearity of the process as

$$\lambda^{(n)} = N\lambda^{(1)}, \tag{11}$$

where (n) denotes the order of the process. Thus in multiphoton absorption processes, the decrease in resolution from the increase in wavelength is compensated only in part by the decrease in the interaction volume due to the nonlinearity of the interaction. Effectively the interaction volume for a N-photon absorption process increases by a factor of $\sqrt{N}$, relative to its single-photon absorption counterpart.

D. The influence of detection

The actual resolution of the microscope is determined not only by the size of the effective interaction volume, but also by the optical configuration of the detection, especially confocal detection, and the coherence properties of the signal. If the effective point spread function of illumination and detection is denoted by psf_{ill} and psf_{det}, respectively, the image formation for an incoherent signal is described by

$$I \propto |psf_{\text{ill}} \cdot psf_{\text{det}}|^2 \otimes O^2, \tag{12}$$

where I and O denote the image and object, respectively, and $\otimes$ denotes a convolution operation. For a fully coherent process on the other hand, Eq. (12) becomes

$$I \propto |psf_{\text{ill}} \cdot psf_{\text{det}} \otimes O|^2. \tag{13}$$

Note that the two imaging modes become identical for a single point object.[67,68] It follows from these equations that in incoherent imaging the object can be thought of as a sum of point sources. The signal of each point source contributing independently to the image. In other words, there is a straightforward and unambiguous relation between object and image. For coherent imaging on the other hand, the imaging characteristics are object dependent, complicating the interpretation of the image. This feature of coherent imaging has recently been addressed in detail for the nonlinear optics microscopy techniques SHG and CARS.[69,70]

As shown above, the effective point spread function for a Nth order nonlinear interaction is in first approximation related to its linear counterpart through

$$psf^{(N)} = [psf^{(1)}]^N. \tag{14}$$

The influence of confocal detection is to suppress out-of-focus signals relative to those from in-focus. Theoretically this results in a multiplication of the excitation point-spread

function with that of the detection. For an infinitely small detection pinhole and a signal wavelength that is equal to that of the fundamental, the influence of the confocal pinhole is to increase the order of the nonlinear process by one:

$$psf^{(N)}_{\text{confocal}} = [psf^{(1)}]^{N+1}. \tag{15}$$

Thus confocal detection reduces the effective interaction volume.

As an example, consider a Nth order multiphoton absorption process, with an excitation wavelength of $N\lambda_{\text{exc}}$, where λ_{exc} is the corresponding single-photon absorption wavelength. Assume further that the fluorescence wavelength $\lambda_{\text{flu}} = N\lambda_{\text{flu}}/\beta$. Then, the size of the effective interaction volume is described by

$$\text{FWHM} = \frac{N}{\sqrt{N+\beta^2}} 2\sigma \sqrt{-2 \ln \frac{1}{2}}. \tag{16}$$

E. Ultrashort pulses

Ultrashort pulses intrinsically have a large optical bandwidth. For transform-limited, Gaussian shaped pulses the time-bandwidth product is given by $\Delta t \cdot \Delta v = 0.44$. The significant bandwidth of ultrashort pulses results in dispersion while propagating through the optical system (see also Sec. IV). This dispersion in turn results in a broadening and distortion of the temporal profile of the pulses. If the induced dispersion is equal for all rays through the optical system it can be compensated for by prechirping, retrieving the minimal pulse width at focus.[41]

More importantly with respect to resolution in nonlinear optical microscopy, is the dispersion that arises from a varying dispersion, including group delay, across the pupil of the microscope objective. This effect is directly related to spherical and chromatic aberrations of the system.[39,71] This leads to a spreading of the optical intensity both in time and in space, which cannot be compensated for in any straightforward manner. To minimize these effects the imaging system should be as achromatic as possible.

F. The influence of noise

In terms of the Rayleigh criterion two, equally bright, object points can just be resolved when the maximum of the intensity distribution of one coincides with the first minimum of the other. In this case, and in the absence of noise, there is a drop of approximately 20% (depending on the shape of the distributions) in the intensity in the image of the two object points. Whether this drop in intensity is detectable in practice depends strongly on the presence of noise. All kinds of noise, e.g., shot noise, thermal noise, read-out noise, photon statistical noise, photon scattering, quantization noise, etc., affect either the background level or the signal's standard deviation and will therefore decrease the signal-to-noise ratio (SNR) of the system. A decrease in SNR in turn decreases the visibility of the drop of the intensity between the maxima as specified by the Rayleigh criterion. Thus the attainable resolution depends not only on the imaging properties of the microscope, i.e., the numerical aperture and the wavelength, but also on the SNR of the image acquisition (Fig. 7).

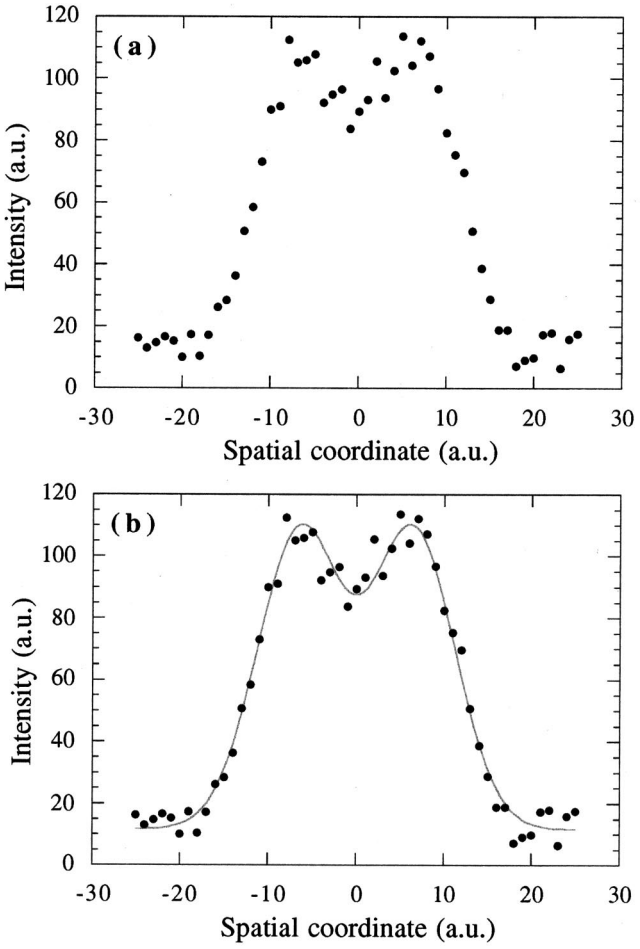

FIG. 7. (a) Intensity profile of two signal point sources, separated according to the Rayleigh criterion, with Poisson noise and 10% detector noise. (b) The use of *a priori* knowledge permits the determination of the position of the two point sources with an accuracy determined by the SNR of the measurement only.

In the special case of a single point object, as, for instance, in the case of single molecule fluorescence imaging, the attainable precision with which the position of the point object can be determined is in fact determined solely by the SNR of the system. In this case it is sufficient to determine the centroid position of the image intensity distribution to localize the object. This situation is analogous to the precision with which the position of stars can be determined using relatively low resolution telescopes.

In general, *a priori* knowledge of the object can be used to increase the attainable resolution of the system. Deconvolution techniques can be applied to limit the influence of noise and limited spatial resolution of the microscope. Alternatively one can argue that the applicability of deconvolution techniques depends strongly on the SNR of the image acquisition.

G. Selected applications

The selected applications presented here are chosen only to illustrate some of the specific features of applying nonlinear optical techniques to high resolution microscopy. It is

outside the scope of this work even to attempt a concise review of this field, which is still expanding at a staggering pace.

The various techniques can be subdivided into two broad categories: (i) ''incoherent'' techniques, in which the induced signal is incoherent and generally emitted randomly in all directions; and (ii) ''coherent'' techniques, where the induced signal is coherent with specific directional and polarization properties. The first category includes the various multiphoton absorption techniques, where the induced signal is incoherent fluorescence. The second category includes a number of wave-mixing techniques such as harmonic generation and stimulated Raman scattering.

1. Applications of incoherent techniques

Squirrell *et al.*[50] have demonstrated that multiphoton absorption microscopy can indeed have advantages in terms of cell viability relative to confocal microscopy. They showed that hamster embryos could be imaged for over 24 h without adverse effects. In these experiments a Nd: YLF laser at 1047 nm and with 175 fs pulses was used. Regular confocal imaging for less than 8 h of the same specimen inhibited development of the embryos even in the absence of fluorophore excitation. For confocal and two-photon absorption microscopy the exposure level was $\sim$280 μJ/embryo and $\sim$2 J/embryo, respectively. It is proposed by the authors that the biological damage induced by confocal microscopy is related to oxidative stress from the photo-induced production of H_2O_2.

Various groups have demonstrated the ability of multiphoton absorption microscopy to image deep into strongly scattering samples. A striking example has been demonstrated in Ref. 3 for *in vivo* two-photon absorption microscopy in the primary vibrissa cortex of anaesthetized rats. Using a 100 fs, $\sim$820 nm Ti: sapphire laser with $<$200 mW of power at the brain dendrites could be resolved down to 500 μm below the pial surface.

The excess power produced by today's laser systems can be used effectively for parallel excitation to increase the image acquisition rate. In 1998, two research groups independently developed two-photon absorption techniques based on multipoint excitation,[58,59] in which multiple points in the object are addressed in parallel. Despite the use of only a standard Ti: sapphire oscillator system in this case, signal levels were large enough to readily view the three-dimensional sectioning through the eye piece of the microscope. Using amplifier laser systems with even higher pulse energies, further parallelization, and consequent increase of the image acquisition rate, is possible. Finally the fluorophore emission capabilities become the limiting factor with ultimate image acquisition rates in the order of 0.1–1 kHz, sufficient to follow, for instance, fast Calcium dynamics in neurons.

2. Applications of coherent techniques

Coherent techniques generally require a different optical setup than incoherent techniques. The coherent nonlinear optical techniques that have so far found their way into high resolution microscopy all generate a coherent signal in the forward direction. Thus in contrast to incoherent techniques where the fluorescence is usually detected in the backscattering direction, signal collection in coherent imaging techniques requires detection of the transmitted signal. The general scheme for this type of microscopy is depicted in Fig. 8. The laser(s) output is focused onto the specimen with a high numerical-aperture microscope objective. The coherent signal is collected in the forward direction by a second objective (or condenser lens) and either imaged directly on a CCD camera or detected by a photomultiplier tube. The specimen is raster scanned using an XY beam scanner, and the specimen stage provides for axial scanning. In general a point-scanning mode is used, although line scanning has been demonstrated[9] to be feasible for high power laser sources in the case of THG imaging.

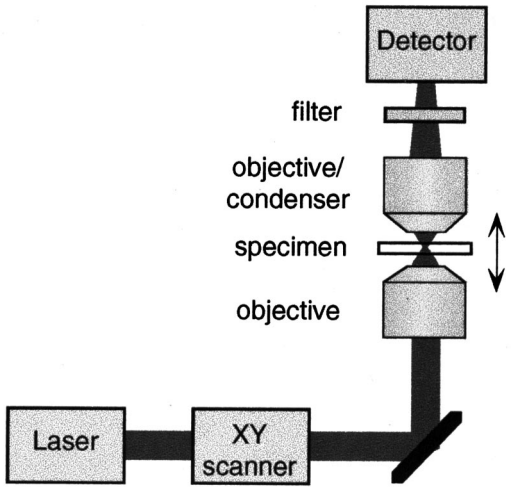

FIG. 8. Schematic of a general coherent nonlinear optics imaging setup. A microscope objective focuses the ultrashort optical pulses (originating from one laser, as in the case of SHG and THG, or from two, as in the case of CARS, lasers) onto the specimen. The specimen is raster scanned in a point excitation mode, generally using mirror scanning for the *X* and *Y* directions and specimen scanning for the *Z* direction. The coherent signal is collected in the forward direction with a second microscope objective or condenser lens. A filter blocks the residual light at the fundamental frequency. The image is collected either directly on a CCD camera or reconstructed after point-by-point detection with a photomultiplier tube.

Some of the specific properties of coherent nonlinear imaging are illustrated below with some selected examples from recent literature. Again it should be stressed that this is in no way a complete overview of the recent advances in this field.

Moreaux and co-workers[72] have exploited the different properties of two-photon absorption and SHG by combining the two techniques simultaneously in a single microscope. In this study use was made of a special fluorophore exhibiting both a significant second-order nonlinear susceptibility and two-photon absorption cross section ($\sim 3\times 10^{-57}\,\mathrm{m^4\,s^2}$ photon^{-1}). Of particular interest for this application is that SHG, in addition to its different specimen symmetry related properties, provides complementary information to two-photon absorption through probing a different nonlinear susceptibility ($\chi^{(2)}$ rather than $\chi^{(3)}$).

The first application of THG microscopy to live cells has been reported by Squier and co-workers.[54] In these experi-

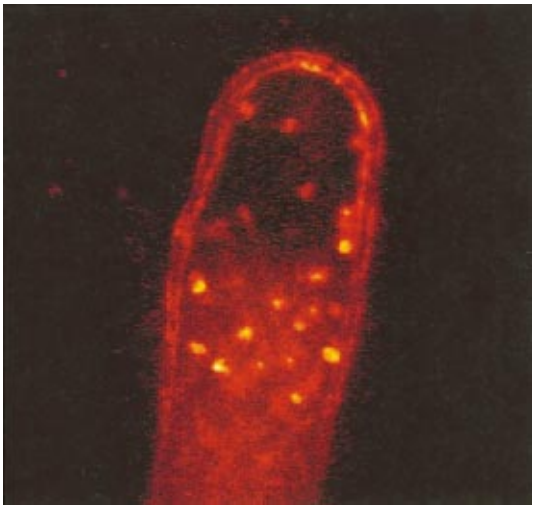

FIG. 9. (Color) THG image of a single optical section of the tip of a rhidzoid from the green alga. The image (image size: $\sim 75 \times 75\ \mu$m) clearly shows the cell wall and the statoliths. The persistence of the strong cytoplasmic streaming and absence of fading of contrast is an indication for the nondisruptive nature of the technique even for times of continuous exposure exceeding 1 h.

ments the nondisruptive behavior of the THG imaging technique was shown for high resolution *in vivo* imaging of the rhizoid from the green alga *Chara* (Fig. 9). Rhizoids are tubular single cells forming the roots of the alga, which have been studied widely especially with respect to their response to gravity. Within the live cell there is a strong cytoplasmic streaming to and from the rhizoid tip. The tip contains so-called statoliths, which are vesicles containing $BaSO_4$ crystals. In *in vivo* imaging the statoliths show dynamic motion while remaining anchored to the actin filament network. No disruption of the cytoplasmic streaming, nor any fading of contrast, has been observed for more than 1 h of continuous exposure; a first indication that the cell remains functional.

In a material sciences application, Yelin and coworkers used an OPO system (130 fs, 1500 nm, 80 MHz) to demonstrate strong phase-matched third-harmonic generation in a nematic liquid crystal cell.[73] Here the optical field can induce its own inhomogeneities in the nonlinear susceptibility by deforming the internal structure of the molecular orientation distribution. Phase-matched THG conversion efficiencies of the fundamental to third harmonic as high as 10^{-5} have been observed in this case.

In another application, Squier and coworkers demonstrated the use of THG imaging to visualize the result of laser-induced breakdown in glass.[53] Using THG, the induced damage can be imaged in three dimensions, providing insight into the effects of exposure levels and duration on the process of laser-induced breakdown. It was demonstrated also that this technique has the potential for reading in optical data storage, where actually the same laser beam at different power levels can be used both for ''writing'' and ''reading'' the data.

A number of recent experiments have demonstrated the potential of CARS microscopy in practice. It has been shown that a folded BoxCARS phasematching configuration can be used at high numerical-aperture imaging conditions, i.e., at high spatial resolution.[74] This permits signal detection with high sensitivity. In parallel experiments, Zumbush and coworkers[75] demonstrated the mild imaging conditions of CARS microscopy by imaging live bacteria and the mitochondria in live HeLa cells.

VII. DISCUSSION

An overview of the basic ultrafast laser sources presently available for performing multiphoton microscopy was presented. These systems are essentially all solid-state, mainly diode-pumped, with average powers on the order of 1 W. The utility of these sources has made multiphoton microscopy a practical method for generating image contrast and has resulted in the further development of a variety of intensity dependent imaging modalities.

The intensity dependence necessitates quantitative knowledge of the microscope dispersion and methods for measuring the pulse width at the focus of the high numerical apertures typically used in imaging. A variety of dispersion compensation schemes as well as methods of pulse measurement for the microscope were discussed. A properly designed dispersion compensation system makes it possible to produce pulse widths well below 50 fs at the focus of the microscope objective.

The resolution aspects of nonlinear optics applications in microscopy have been discussed. In general the interaction volume in the specimen decreases with an increasing order of nonlinearity of the process. In multiphoton absorption processes this tendency is counterbalanced by a relative increase in excitation wavelength. Importantly, it was shown that the optical transfer function for coherent type processes is, in contrast to that for incoherent processes, object dependent.

A number of applications of nonlinear optics microscopy have been presented, ranging from applications in the field of the material sciences to *in vivo* biology. Two-photon absorption microscopy is already widely accepted as a valuable imaging tool, especially in biology. More recently a number of coherent nonlinear optics techniques, such as harmonic generation and stimulated Raman, have been applied to high resolution imaging. Given the status of laser development, it is to be expected that a whole range of nonlinear optical spectroscopic techniques will be implemented in, and utilized for, high resolution microscopy.

ACKNOWLEDGMENTS

J. S. would like to acknowledge Dr. David Fittinghoff for preparation of the interferometric autocorrelation figures. J. S. would also like to acknowledge support from the National Science Foundation, Grant No. DBI-9987257.

[1] W. Denk, J. H. Strickler, and W. W. Webb, Science **248**, 73 (1990).
[2] W. Denk, Proc. Natl. Acad. Sci. U.S.A. **91**, 6629 (1994).
[3] K. Svoboda *et al.*, Nature (London) **385**, 161 (1997).
[4] R. Gauderon, P. B. Lukins, and C. J. R. Sheppard, Opt. Lett. **23**, 1209 (1998).
[5] P. J. Campagnola *et al.*, Biophys. J. **77**, 3341 (1999).
[6] M. D. Duncan, J. Reijntjes, and T. J. Manuccia, Opt. Lett. **7**, 350 (1982).
[7] M. D. Duncan, Opt. Commun. **50**, 307 (1984).
[8] Y. Barad *et al.*, Appl. Phys. Lett. **70**, 922 (1997).
[9] M. Müller *et al.*, J. Microsc. **191**, 266 (1998).

[10] D. E. Spence, P. N. Kean, and W. Sibbett, Opt. Lett. **16**, 42 (1991).
[11] D. Kopf *et al.*, Opt. Lett. **22**, 621 (1997).
[12] K. Svoboda *et al.*, Opt. Lett. **21**, 1411 (1996).
[13] J. M. Girkin, D. Burns, and M. D. Dawson, Proc. SPIE 92 (1999).
[14] D. Kopf *et al.*, Appl. Phys. B: Lasers Opt. **B65**, 235 (1997).
[15] D. L. Wokosin and J. G. White, Proc. SPIE 25 (1997).
[16] D. L. Wokosin *et al.*, IEEE J. Sel. Top. Quantum Electron. **2**, 1051 (1996).
[17] D. Kopf *et al.*, Opt. Lett. **20**, 1169 (1995).
[18] J. Aus der Au *et al.*, Opt. Lett. **23**, 271 (1998).
[19] A. Robertson *et al.*, J. Opt. Soc. Am. B **17**, 668 (2000).
[20] M. Hofer *et al.*, IEEE Photonics Technol. Lett. **11**, 650 (1999).
[21] M. E. Fermann, Opt. Lett. **23**, 52 (1998).
[22] A. Galvanauskas *et al.*, Opt. Lett. **22**, 105 (1997).
[23] A. C. Millard *et al.*, Appl. Opt. **38**, 7393 (1999).
[24] K. R. Wilson and V. V. Yakovlev, J. Opt. Soc. Am. B **14**, 444 (1997).
[25] T. Wilhelm, J. Piel, and E. Ridle, Opt. Lett. **22**, 1494 (1997).
[26] A. Baltuska *et al.*, Appl. Phys. B: Lasers Opt. **B65**, 175 (1997).
[27] E. O. Potma *et al.*, Opt. Lett. **23**, 1763 (1998).
[28] D. Strickland and G. Mourou, Opt. Commun. **56**, 219 (1985).
[29] C. P. J. Barty, B. E. Lemoff, and C. L. Gordon III, Proc. SPIE 6 (1993).
[30] M. Müller, J. Squier, and G. J. Brakenhoff, Opt. Lett. **20**, 1038 (1995).
[31] J. K. Ranka *et al.*, Opt. Lett. **22**, 1344 (1997).
[32] A. C. Millard *et al.*, J. Microsc. **193**, 179 (1999).
[33] T. Jasapara and W. Rudolph, Opt. Lett. **24**, 777 (1999).
[34] T. Y. F. Tsang, Phys. Rev. A **52**, 4116 (1995).
[35] D. Meshulach, Y. Barad, and Y. Silberberg, J. Opt. Soc. Am. B **14**, 2122 (1997).
[36] J. A. Squier *et al.*, Opt. Commun. **147**, 153 (1998).
[37] R. Trebino *et al.*, Rev. Sci. Instrum. **68**, 3277 (1997).
[38] D. N. Fittinghoff *et al.*, IEEE J. Quantum Electron. **35**, 479 (1999).
[39] Z. Bor, Opt. Commun. **94**, 249 (1992).
[40] C. Radzewicz, M. J. la Grone, and J. S. Krasinski, Opt. Commun. **126**, 185 (1996).
[41] M. Müller *et al.*, J. Microsc. **191**, 141 (1998).
[42] J. B. Guild, C. Xu, and W. W. Webb, Appl. Opt. **36**, 397 (1997).
[43] S. Kane and J. Squier, IEEE J. Quantum Electron. **31**, 2052 (1995).
[44] S. Kane *et al.*, Proc. SPIE 183 (1996).
[45] W. H. Knox *et al.*, Opt. Lett. **13**, 574 (1988).
[46] K. König *et al.*, Opt. Lett. **22**, 135 (1997).
[47] K. König *et al.*, Opt. Lett. **24**, 113 (1999).
[48] J. A. Curcio and C. C. Petty, J. Opt. Soc. Am. **41**, 302 (1951).
[49] A. Schönle and S. W. Hell, Opt. Lett. **23**, 325 (1998).
[50] J. M. Squirrell *et al.*, Nat. Biotechnol. **17**, 763 (1999).
[51] C. B. Schaffer, N. Nishimura, and E. Mazur, Proc. SPIE 2 (1998).
[52] C. B. Schaffer *et al.*, Proc. SPIE 36 (1998).
[53] J. Squier and M. Müller, Appl. Opt. **38**, 5789 (1999).
[54] J. Squier *et al.*, Opt. Express **3**, 315 (1998).
[55] G. J. Brakenhoff *et al.*, J. Microsc. **181**, 253 (1996).
[56] E. H. K. Stelzer *et al.*, Opt. Commun. **104**, 223 (1994).
[57] M. Petrán *et al.*, J. Opt. Soc. Am. **58**, 661 (1968).
[58] A. H. Buist, M. Müller, and G. J. Brakenhoff, J. Microsc. **192**, 217 (1998).
[59] J. Bewersdorf, R. Pick, and S. W. Hell, Opt. Lett. **23**, 655 (1998).
[60] D. N. Fittinghoff and J. A. Squier, Opt. Lett. **25**, 1213 (2000).
[61] D. N. Fittinghoff, P. W. Wiseman, and J. A. Squier, Opt. Express **7** (2000).
[62] M. A. A. Neil, M. J. Booth, and T. Wilson, Opt. Lett. **23**, 1849 (1998).
[63] M. A. A. Neil *et al.*, J. Microsc. **200**, 105 (2000).
[64] O. Albert *et al.*, Opt. Lett. **25**, 52 (2000).
[65] M. Born and E. Wolf, *Principles of Optics*, 6th ed. (Pergamon, Oxford, 1980).
[66] J. J. Stamnes, *Waves in Focal Regions* (IOP, Bristol, 1986).
[67] J. W. Goodman, *Introduction to Fourier Optics* (McGraw-Hill, New York, 1968).
[68] J. Deitche, M. Kempe, and W. Rudolph, J. Microsc. **174**, 69 (1994).
[69] L. Moreaux, O. Sandre, and J. Mertz, J. Opt. Soc. Am. B **17**, 1685 (2000).
[70] E. O. Potma, W. P. de Boeij, and D. A. Wiersma, J. Opt. Soc. Am. B **17**, 1678 (2000).
[71] M. Kempe *et al.*, J. Opt. Soc. Am. B **9**, 1158 (1992).
[72] L. Moreaux *et al.*, Opt. Lett. **25**, 320 (2000).
[73] D. Yelin *et al.*, Phys. Rev. Lett. **82**, 3046 (1999).
[74] M. Müller *et al.*, J. Microsc. **197**, 150 (2000).
[75] A. Zumbusch, G. R. Holtom, and X. S. Xie, Phys. Rev. Lett. **82**, 4142 (1999).